Journal of Materials Chemistry

Cite this: *J. Mater. Chem.*, 2011, **21**, 15224

www.rsc.org/materials

PAPER

In situ measurement of power conversion efficiency and molecular ordering during thermal annealing in P3HT:PCBM bulk heterojunction solar cells†

Neil D. Treat,[ab] Chris G. Shuttle,[b] Michael F. Toney,[d] Craig J. Hawker*[abc] and Michael L. Chabinyc*[ab]

Received 10th June 2011, Accepted 1st August 2011
DOI: 10.1039/c1jm12677f

Bulk heterojunction organic solar cells hold much promise as commercially viable sources of renewable energy due to their relatively inexpensive fabrication. Developing a fundamental knowledge of how processing conditions influence solar power conversion efficiency will enable rational and efficient design, optimization, and control of new organic solar cell materials. In this report, we use a combination of *in situ* current–voltage measurements and grazing-incidence wide-angle X-ray scattering experiments at elevated temperature to correlate the changes in photoconversion efficiency to the changes in the molecular ordering of a poly(3-hexylthiophene):[6,6]-phenyl-C_{61}-butyric acid methyl ester (P3HT:PCBM) bulk heterojunction active layer. *In situ* measurements of current–voltage characteristics were used to optimize the power conversion efficiency and the resulting thermal processing was in agreement with studies from repeated heating and cooling cycles. The improvements in short circuit current with thermal annealing were correlated to an increase in the population of face-on oriented crystallites of P3HT rather than improvements in molecular ordering of PCBM.

1. Introduction

Organic thin film solar cells hold significant potential as part of a future renewable energy portfolio due to their recent improvements in efficiency to ~8%.[1] The most efficient structure for single layer organic photovoltaic devices comprises a blend of electron donating and accepting materials cast from a common solvent forming a bulk heterojunction (BHJ).[2] Significant improvements in the photoconversion efficiency of BHJs have been accomplished through the development of new electron-donating polymers that more efficiently absorb the solar spectrum. Further improvements have been accomplished by optimizing the processing conditions that influence the active layer morphology (*i.e.* phase separation and molecular ordering).[1,3] In order to increase the power conversion efficiency to 10%, which is an economically important benchmark, it is essential to develop a better understanding of how the molecular ordering of the active layer affects the electronic properties.

The most extensively studied BHJ is a mixture of an electron-donating polymer, poly(3-hexylthiophene) (P3HT), and electron-accepting fullerene, [6,6]-phenyl-C_{61}-butyric acid methyl ester (PCBM).[4–6] The photoconversion efficiency has a strong dependence on a large number of material (*e.g.* molecular weight) and processing parameters (*e.g.* annealing conditions).[6–9] Thermal treatment has been shown to improve the efficiency of P3HT:PCBM BHJ solar cells, with significant effort focused on determining the timescales and temperatures needed to produce the most efficient organic solar cells.[6,9] Some prior studies suggest that the improvement in device performance is due to the increase in the total P3HT crystallinity and development of PCBM nanocrystallites or aggregates.[10,11]

The majority of studies aimed at discovering the connection between morphology and power conversion efficiency (PCE) have focused on the static picture of the state of the BHJ before and after thermal annealing.[4,6,12] Recently there have been a number of *in situ* studies of morphological changes that are beginning to unlock the dynamics of thermal annealing in P3HT:PCBM BHJs.[13,14] Specifically, it has been found that the total population of P3HT crystallites increases with annealing, but the PCBM remains predominately amorphous (correlation length of ~2 nm) during thermal annealing process.[12–14] The results of these studies have been used to rationalize the changes in PCE after the annealing process and have found that increases in P3HT ordering and other morphological factors are associated with higher performance.

Herein, we use a combination of temperature controlled two-dimensional grazing-incidence wide-angle X-ray scattering, (GIWAXS)[13] and current–voltage (J–V) measurements to investigate the effects of molecular ordering on the photoconversion efficiency. In contrast to previous studies, we measure

[a]*Materials Research Laboratory, University of California Santa Barbara, Santa Barbara, CA, USA*
[b]*Materials Department, University of California Santa Barbara, Santa Barbara, CA, USA*
[c]*Department of Chemistry and Biochemistry, University of California Santa Barbara, Santa Barbara, CA, USA*
[d]*Stanford Synchrotron Radiation Lightsource, SLAC National Accelerator Laboratory, Menlo Park, CA, USA*
† Electronic Supplementary Information (ESI) available: See DOI: 10.1039/c1jm12677f

the evolution of the PCE as a function of time during the thermal annealing process rather than after cooling to room temperature. The correlation of these two techniques at elevated temperatures allows for an opportunity to gain insight into the evolution of the molecular ordering of the active layer and its impact on charge generation and transport. We observe that the photoconversion efficiency improves most rapidly within the first 5 min of annealing when held at a constant temperature (90 °C), which corresponds to an increase in the population of face-on oriented P3HT crystallites. By measuring the J–V characteristics while increasing the temperature at a constant rate, we show the PCE to be highest at 150 °C for this system, which is in good agreement with previous studies.[5,6,15] We relate this improvement in photoconversion efficiency to the increase in the relative population of face-on oriented P3HT crystallites and the total degree of P3HT crystallinity. There was little connection between improvement in the photoconversion efficiency and the change in molecular ordering of PCBM at annealing temperatures below 170 °C (since there were insignificant changes in the PCBM X-ray scattering). However, micron-scale PCBM crystallites were observed upon heating for longer periods of time at 180 °C, which was correlated to the degradation in photoconversion efficiency as observed by many others.[7,16,17] This observation leads to the conclusion that PCBM forms a percolation pathway of highly disordered domains in efficient P3HT:PCBM BHJs. Note that X-ray diffraction does not allow for the investigation of the morphology of disordered P3HT and PCBM domains even though this morphology will effect the photoconversion efficiency. Importantly, this study allows for the changes in current–voltage characterisitcs during heating to be separated into contributions from morphological changes and simple effects due to activated transport.

2. Experimental

Materials

Poly(3-hexylthiophene) and [6,6]-phenyl-C_{61}-butyric acid methyl ester (99.5%) were used as received from Merck Chemicals and Nano-C respectively.

Device fabrication and testing

ITO-coated glass substrates were ultrasonicated in acetone, 2% soap in water, deionized water, and 2-propanol for 20 minand dried with nitrogen. A 40 nm thick film of PEDOT:PSS (Clevios PH500) was deposited by spin coating at 4000 rpm for 40 s and dried at 165 °C for 10 min. The P3HT:PCBM solutions (1 : 0.8 by weight) were prepared with a total concentration of 18 mg mL^{-1} in chlorobenzene and stirred overnight at 70 °C. The BHJ solution was deposited in a N_2 filled glove box on the prepared substrates at 700 rpm for 40 s and 2000 rpm for 5 s yielding an active layer thickness of ~70 nm. A 100 nm thick Al anode (0.06 cm^2) was then deposited by thermal evaporation under vacuum (<10^{-6} torr).

The P3HT:PCBM BHJ solar cells were illuminated by an array of 14 green 1W LumiLEDs mounted directly above the center of a digitally controlled hotplate in a N_2 filled glove box. A P3HT:PCBM BHJ was attached to a glass slide mounted on a metal plate and was electrically connected using a dip-clip. The temperature of the solar cells was measured by a thermocouple attached to the glass slide positioned adjacent to the solar cell. The temperature of the glass slide was continually measured, and was used as an estimate of the solar cell temperature. For the controlled temperature ramp studies, the metal plate with the device mounted was placed on the hotplate set at room temperature, with the ITO side facing upwards. The hotplate was then set with a temperature ramp of 4 °C per min and *J–V* curves were then measured in a light/dark sequence using a Keithley 2400 SMU.

For the constant temperature measurements, a metal plate with attached glass slide was preheated on the hotplate. The metal plate was removed, and the solar cell was quickly attached to the glass slide, before placing it back on the hotplate. *J–V* curves were then continually measured as previously described. The glass slide rose to the desired annealing temperature within approximately 2 min.

Grazing incidence wide angle X-Ray scattering

2D GIWAXS experiments were performed at the Stanford Synchrotron Radiation laboratory on beamline 11–3 with an area detector (MAR345 image plate) at an incident energy of 12.7 keV. The samples were kept under a helium atmosphere during irradiation to minimize X-ray beam damage. Films were typically exposed for 60 s at a grazing incidence angle of 0.12°. For the constant temperature measurements, the stage was preheated to temperature, then the film was placed on the stage and allowed to equilibrate for a minimum of 2 min before investigation. For the temperature ramp studies, the scattering profile was measured at 10 °C increments with a 10 °C per min heating rate. Note that stage alignment and collection took approximately 5 min, which closely replicates the 3 °C min^{-1} heating conditions used in the J–V measurements.

3. Results and discussion

All films in this study were fabricated using a P3HT:PCBM (1 : 0.8 by wt.) solution with a concentration of 18 mg mL^{-1} (based on total weight) in chlorobenzene (fabrication detailed in experimental section) yielding an active layer thickness of approximately 70 nm. This active layer thickness was chosen to reduce the probability of bimolecular recombination. Thinner active layer films increase the average electric field, which reduces the free charge carrier transit time due to the dependence on thickness squared. The reduction in the probability of bimolecular recombination also conveniently minimizes the effects of temperature dependent mobility on the photoconversion efficiency (as demonstrated below). All samples used in this study were fabricated from the same solution concentration and fabrication conditions, which allow for direct comparison between the photovoltaic cells and the GIWAXS samples. The mean photoconversion efficiency of the P3HT:PCBM BHJ solar cells was 2.3% and 4.5% with Al and LiF/Al electrodes respectively (Figure S1). All studies were performed on devices with Al electrodes due to the commonly observed decrease in the photoconversion efficiency observed when heating devices with LiF/Al electrodes.

Kinetics of annealing

A relatively low temperature (90 °C) was initially selected, which is less than typically used to thermally anneal P3HT:PCBM solar cells. Heating at a lower temperature reduces the BHJ reorganization kinetics (PCBM and P3HT diffusion and crystallization), which allows us to determine the maximum time needed before no further changes in device performance are observed.[18,19] Higher temperatures (150 °C) increase the rate of change in the active layer morphology, which slightly increases the rate of change in the photoconversion efficiency with time (Figure S2). These isothermal measurements allow us to separate the effects of the temperature dependent charge transport (reversible upon cooling) and changes in BHJ morphology (irreversible upon cooling) on the photoconversion efficiency. In general, an increase in temperature will tend to improve the carrier mobility of organic semiconductors due to thermally activated de-trapping as long as there are no dramatic changes in structure.[20] For example, at a phase transition where the ordering changes dramatically, *e.g.* near a melt, the mobility may begin to decrease due to the competition between thermal activation for hopping and a broadening of the DOS.[21]

By using *in situ* J–V measurements, it was determined that the most significant changes in the PCE occurred within the first 5 min of heating at 90 °C. Fig. 1a–c shows the real-time light and dark J–V curves and the corresponding device characteristics of a P3HT:PCBM BHJ heated to 90 °C. It takes approximately two minutes for the device to reach the targeted temperature, so only the J–V characteristics after two minutes are reported. Any changes in the device characteristics after this time are dominated by temperature dependent changes in the active layer morphology. All times reported are after the device has reached 90 °C. The most significant improvement in photoconversion efficiency occurred within the first 5 min of annealing (only a 5% change in the photoconversion efficiency after an addition 25 min of heating at 90 °C). Specifically, the short-circuit current density (J_{sc}) and fill-factor (FF) both increase by approximately 25% and 15% of the original value in the first 5 min, whereas the open-circuit voltage (V_{oc}) continues to decrease until the value plateaus after nearly 20 min of heating. Further analysis revealed that the increase in the J_{sc} observed during the isothermal measurements follows a stretched exponential function for all temperatures investigated (Figure S3).[13] Note that the value for the J_{sc} was not corrected for the slight change in spectral absorption observed in P3HT upon heating to 90 °C.[22]

Additionally, the dark current under forward bias increases with increasing annealing time (Fig. 1b). This increase signifies a decrease in series resistance in the device, which is likely due to the improvement in molecular ordering of the P3HT upon annealing as discussed below. It was also found that the V_{oc} in these devices decreased by ~20% to an average value of 0.50 V when measured at 90 °C. Following the standard circuit model for a solar cell (a diode in parallel with a current generator), a decrease in V_{oc} is expected when the dark current under forward bias increases (decrease in series resistance).

Thus, by using *in situ* current–voltage measurements of P3HT:PCBM BHJ solar cells, it was determined that the photoconversion efficiency improved primarily within the first 5 min of annealing at 90 °C. It should be made clear that upon cooling to room temperature, the improvement in the J_{sc} and the FF was retained.

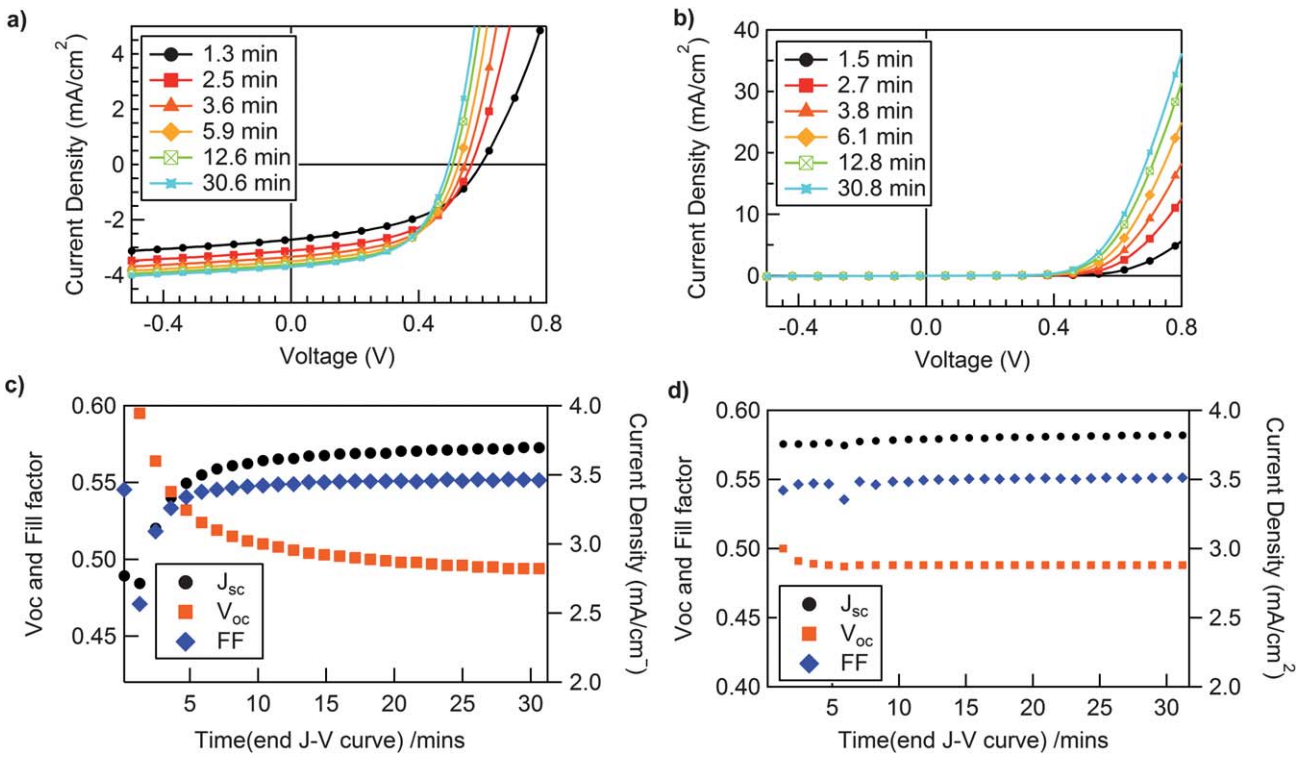

Fig. 1 a) Light and b) dark current–voltage measurements of an as-cast P3HT:PCBM device measured at 90 °C. c) J_{sc}, V_{oc}, and FF of the same device as a function of time heated at 90 °C. d) Measurement of the J_{sc}, V_{oc}, and FF of a device which had been previously annealed at 90 °C for 20 min as a function of time heated at 90 °C.

This observation is consistent with previous reports that used sequentially annealed P3HT:PCBM BHJ devices measured at room temperature.[6,23] For the devices used in this study, it was concluded that all dominant changes in the phase separation and molecular ordering of the active layer that influence the photoconversion efficiency likely occur in a fraction of the time commonly used to thermally anneal P3HT:PCBM BHJs (30 min). It should be noted that the J_{sc} continues to increase with increasing annealing temperature, and it is probable that a different equilibrium structure is reached at these different temperatures (as seen in Fig. 4). However, in practice, the increase in annealing temperature only slightly increases the rate of change in the device characteristics (Figure S2).

Next, a pre-annealed device was reheated to 90 °C in order to ensure that the increase in photoconversion efficiency was solely due to irreversible changes in the molecular ordering of the active layer and not from reversible temperature dependent changes in the active layer morphology or charge transport. The J–V characteristics (Fig. 1d) measured at 90 °C as a function of time reveal that there is little change in the J_{sc}, FF, or V_{oc} with time (<2%). This demonstrates that the enhancement in the device performance initially observed is an irreversible change, which is attributed to the improvement in the molecular ordering and phase separation of the P3HT:PCBM BHJ and is once again consistent with previous studies using sequential annealing.[5,6,12,23]

Changes in the molecular ordering of the active layer at 90 °C as a function of time were probed at the Stanford Synchrotron Radiation Lightsource beam line 11–3, which is equipped with a 2D image plate detector (2D GIWAXS) and a temperature controlled stage.[13] Note that all scattering experiments utilized samples without a top electrode, which is the most commonly used sample structure. Recently, a study of P3HT:PCBM BHJs annealed with and without deposited electrodes showed that the absence of the confining effects of the top electrode may decrease the relative population of face-on oriented P3HT crystallites.[24] For this experiment, the X-ray incidence angle was chosen such that the bulk of the P3HT:PCBM film was probed. The scattering vectors in the out-of-plane and in-plane direction are denoted as $\mathbf{q_z}$ and $\mathbf{q_{xy}}$ respectively. 2D diffraction patterns of an as-cast P3HT:PCBM film, annealed at 90 °C for 5 min, and upon cooling to room temperature after heating at 90 °C for 20 min can be seen in Figure S4. For ease of interpretation, integrated cake slices along the meridian and horizon of the 2D diffraction patterns are reported in Fig. 2. For the as-cast P3HT:PCBM BHJ (measured at 25 °C), the characteristic diffraction peaks for the (100), (200), and (300) (packing along the side chains or *a*-axis) of a P3HT crystallite are found near the meridian and horizon (near $\mathbf{q_z}$ and $\mathbf{q_{xy}}$) at $\mathbf{q}$ = 0.39, 0.77, 1.15 Å^{-1}, respectively, and weak diffraction from the (020) (π-stacking direction or *b*-axis) near the horizon and meridian (along $\mathbf{q_{xy}}$ and $\mathbf{q_z}$) at $\mathbf{q}$ = 1.65 Å^{-1}. Note that the peaks along the meridian are not exactly along $\mathbf{q_z}$, due to the intersection of the flat 2D detector with the Ewald sphere in the grazing incidence geometry.[25] The peak placement in the diffraction pattern of an as-cast P3HT:PCBM BHJ reveals that there is a mixed orientation of P3HT crystallites (Fig. 3b). The diffuse ring centered at $\mathbf{q}$ = 1.41 Å^{-1} is due to scattering from weakly correlated PCBM molecules.[12,13,18] The PCBM phase is determined to be highly disordered because the peak width of PCBM scattering ring corresponds to a correlation length of roughly 2 nm (two PCBM molecules) as determined using Scherrer's equation (detailed in the supporting informtion).

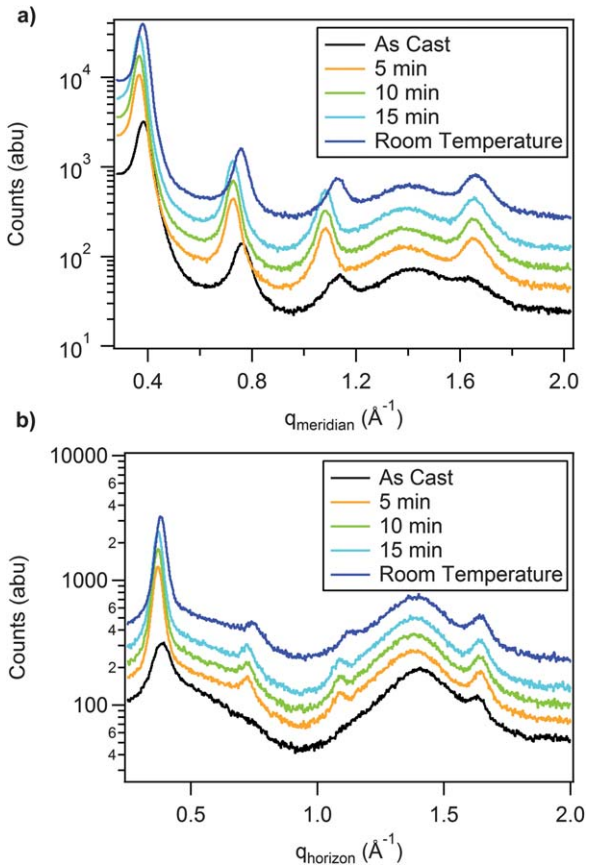

Fig. 2 Cake slices from a 2D GIWAXS diffraction pattern of a P3HT:PCBM BHJ a) along the meridian b) along the horizon. Patterns were collected from an as-cast sample (black), measured at 90 °C after annealing for 5 min (orange), 10 min (green), and 15 min (aqua). The blue trace represents a sample measured at room temperature after annealing for 20 min at 90 °C. Curves are offset for clarity.

As the sample is heated to 90 °C, the P3HT (h00) and (0k0) diffraction peak intensities increase. Further analysis of the GIWAXS patterns reveals upon thermal annealing, there is an increase in the total number of P3HT crystallites (Figure S5) as well as the crystallite thickness along the *a*-axis (Table S3). Note that upon heating, peaks shift to lower values of $\mathbf{q}$ due to the thermal expansion within the P3HT crystallites.[13] Most notably,

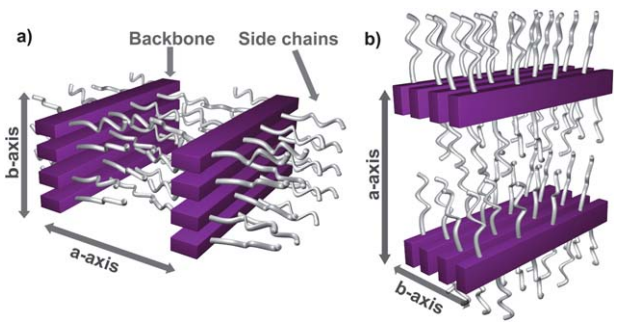

Fig. 3 Graphical representation of a P3HT crystallite oriented a) face-on and b) edge on. The purple block represents the thiophene backbone and white cylinders the hexyl side chains.

there is the observed increase in the ratio between the diffraction intensity of the (020) reflection occurring near the meridian and the horizon at $\mathbf{q} = 1.65$ Å^{-1}. This change is accompanied by a decrease in the ratio of the (h00) reflections found near the meridian and horizon (Figure S3). The ratio between the *b*-axis along the meridian and *a*-axis along the horizon corresponds to the increase in P3HT crystallite population having the π-stacking oriented perpendicular to the substrate and alkyl chains parallel, thus having a face-on crystallite orientation (Fig. 3a). It should be noted that the increase in face-on oriented P3HT crystallites is also consistent with GIWAXS of pre-annealed P3HT:PCBM BHJs measured at room temperature.[12,24] The disagreements with other *in situ* studies most likely occur because different film thicknesses, casting solvents, and batches of P3HT were used.[13]

Significantly, the distribution of the scattering ring corresponding to highly disordered PCBM at $\mathbf{q} = 1.41$ Å^{-1} remains unchanged and the intensity slightly decreases during the annealing process, thus signifying that the molecular ordering of PCBM changes very little during the thermal annealing (Figure S5c). This observation may be surprising considering that PCBM can diffuse relatively easily through disordered P3HT (~220 nm per *sec*)[18,19,24] suggesting that growth of PCBM crystalline domains does not occur in our times (30 min) at these temperatures.

Our results show that the most significant changes in the molecular ordering of the P3HT crystallites and device performance occur during the first 5 min of heating at 90 °C. Relating this information to the *in situ* J–V measurements leads us to believe that all relevant morphological transformations in P3HT:PCBM BHJ devices are completed after only 5 min of annealing at 90 °C. In many studies, the annealing time at each step is arbitrarily chosen; one can easily imagine cases (*e.g.* optimizing new materials) where the time is too long leading to degradation in the photoconversion efficiency.

The increase in the J_{sc} and FF is believed to result from the increase in the population of face-on orientated P3HT crystallites, and that there is little change in the ordering of the PCBM within the active layer upon thermal annealing. Our data supports the idea that the increase in the face-on oriented P3HT crystallites of the P3HT is the dominant factor that reduces the contact resistance between the active layer and electrodes. This change also reduces the series resistance within the film due to more efficient vertical charge transport within these devices. Additionally, there was an increase in the total P3HT crystallite population (as evident in Figure S5). This also increases the charge carrier mobility and light absorption of the BHJ, both of which improve the FF and J_{sc}.

Optimization of annealing time and temperature

The J–V characteristics of an as-cast P3HT:PCBM BHJ device was also measured while increasing the temperature by approximately 3 °C/min. This study was performed so that the changes in the P3HT:PCBM BHJ device characteristics at different annealing temperatures could be correlated to the changes in molecular ordering. A sufficiently slow ramp rate was chosen so that the device performance was not limited by the P3HT crystallization kinetics (as previously determined from the constant temperature J–V measurements). Note that in this case, the changes in J–V characteristics with temperature represent both temperature dependent changes on charge transport and injection as well as changes in the molecular ordering of the active layer.[26] As the temperature was increased from room temperature, a shallow local maximum in the J_{sc} was observed at ~35 °C (Fig. 4a). Additionally, a shallow local maximum for the dark current under forward bias was also observed at the same temperature (Fig. 4b). The observed local maxima for the J_{sc} and dark current may be related to changes in the blend morphology as the active layer is taken above the glass transition temperature.[27] As the device temperature was increased above 50 °C, the dark current, J_{sc}, and FF strongly increase, whereas the V_{oc} and series resistance both decrease (Fig. 4). The temperature at which the device characteristics begin to rapidly (50 °C) change agrees well with the onset of appreciable diffusion of PCBM in P3HT.[18] The broad maximum for the J_{sc}, FF, and dark current occurred at approximately 150 °C, coinciding with a minimum value for the series resistance (estimated from the slope in the darkcurrent at 1.5V). As the temperature was increased above 150 °C, the J_{sc}, FF, and dark current began to decrease. Note that the blue-shift in the P3HT absorption spectra becomes more pronounced with increasing temperature.[24] The J_{sc} is expected to decrease by ~6% at temperature based on an estimate of the overlap of the emission of the green LED and the absorption spectrum of the blend at 150 °C (Figure S9). With consideration of this small difference, we find an optimal temperature of 150 °C from the *in situ* studies that is in good agreement with most studies of P3HT:PCBM

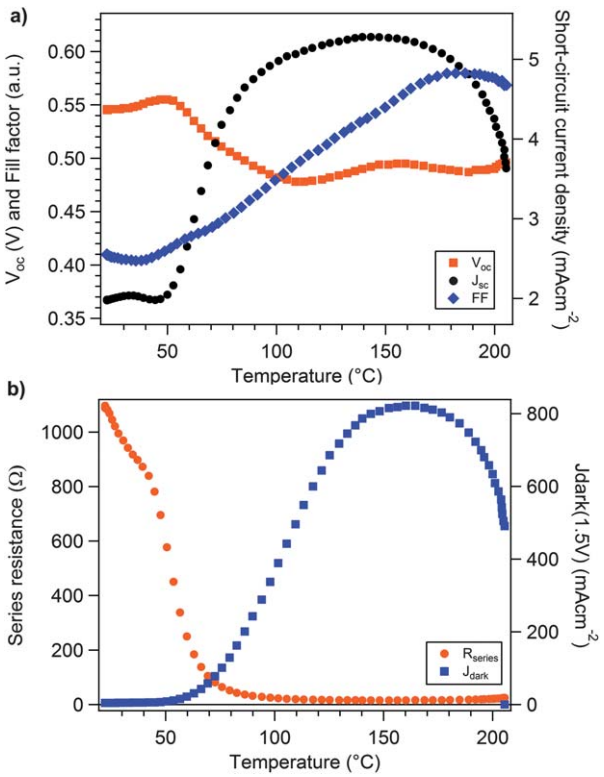

Fig. 4 a) J–V characteristics of an as-cast P3HT:PCBM BHJ as a function of temperature: J_{sc}(black circle), FF (blue diamond), and V_{oc}(orange square) b) series resistance (blue squares) and dark current (orange circles) measured under illumination for a P3HT:PCBM BHJ solar cell as the temperature is increased by 3 °C/min. The series resistance was estimated by the slope in the dark current at 1.5V.

solar cells from repeated cycles of heating and cooling or by testing multiple devices.[6] It should be noted that all the observed improvements in the photoconversion efficiency were retained when the device was cooled to room temperature from 150 °C. It is generally assumed that the improvement in the photoconversion efficiency when annealing *via* continuous heating or cycling is equivalent. However, this effect may not be general to all polymer:fullerene systems that improve upon annealing.[6,9]

Next, a P3HT:PCBM BHJ device that was previously annealed for 10 min at 150 °C was heated using the same profile reported above so that the changes in charge transport and injection with temperature (reversible changes) could be distinguished from the irreversible changes in the molecular ordering of the BHJ (Fig. 5). It was found that the J_{sc} and FF are independent of temperature below 150 °C and the V_{oc} decreased by 200 mV. In general, an increase in temperature will improve the carrier mobility of organic semiconductors due to thermally activated de-trapping effects.[20] Thus, we would expect an increase in the current under forward bias (decrease in series and contact resistance) and an increase in the J_{sc} and FF if either geminate or non-geminate recombination losses are present.[28] Consequently, it is also expected that the increase in current under forward bias and FF will lead to a decrease in the V_{oc}. Because there is little change in J_{sc} and FF with an increase in temperature (below 150 °C), we are led to believe that these thin devices have little non-geminate recombination losses. Previous studies have shown that PCBM can move up to ~220 nm per second in P3HT:PCBM films at these temperatures;[18,19] thus it is surprising that the diffusion of PCBM has little effect on the device characteristics (increasing molecular mobility should increase the energetic disorder). These observations allow us to confirm that the improvement in efficiency observed upon initial heating during *in situ* characterization is dominated by improvement in the molecular ordering of the P3HT:PCBM BHJ, which was not reversed upon cooling to room temperature rather than a simple effect such as activated charge transport. Recent work has suggested that the rapid cooling rate from 150 °C causes a decrease of ~5% relative to slower cooling and was attributed to a reduction in optical density due to increased disorder.[29] We have not examined the impact of the cooling rate here.

At temperatures above 170 °C, the J_{sc} and FF sharply decreased, which was accompanied by a slight increase in the V_{oc} (due to the increase in series resistance) (Fig. 5). The changes in V_{oc} and the dark current under forward bias are consistent with the standard model for the solar cell (as discussed above). Our data suggests that this decrease in photoconversion efficiency is due to deleterious changes in the phase separation (*i.e.* formation of micron-scale crystalline domains of PCBM). This conclusion is supported by the combination of 2D GIWAXS diffraction patterns and the observation of large aggregates with optical microscopy (data presented below) and is consistent with observations made in other reports.[7,30] Note that the time scales and temperatures at which micon-scale PCBM aggregation occurs may vary due to inconsistent material and processing parameters (*e.g.* residual solvent[31]).

Again, the evolution in the molecular ordering of the active layer upon thermal annealing was investigated using 2-D GIWAXS. The GIWAXS data presented were collected from

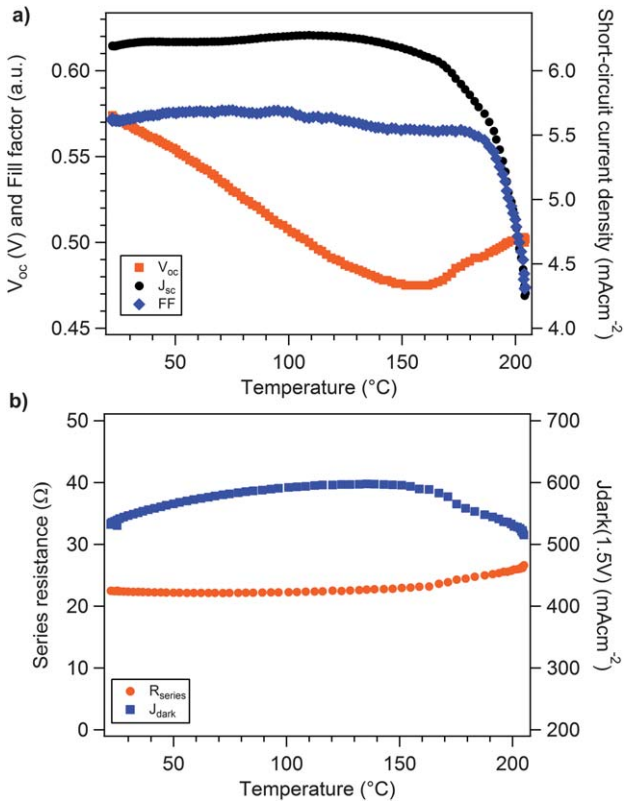

Fig. 5 a) J–V characteristics of a P3HT:PCBM BHJ previously annealed at 150 °C for 20 min. as a function of temperature: J_{sc}(black circle), FF (blue diamond), and V_{oc}(orange square) b) series resistance (blue squares) and dark current (orange circles) measured under illumination for a P3HT:PCBM BHJ solar cell as the temperature is increased by 4 °C/min. The series resistance is estimated by the slope in the dark current at 1.5V.

a single sample that was heated at a rate of 30 °C min^{-1} and held every 10 °C for 4 min thus closely replicating the change in temperature used to probe the change in photoconversion efficiency (Fig. 4). Scattering data from an as-cast P3HT:PCBM BHJ measured at 90 °C, 120 °C, 150 °C, and 180 °C are presented in Fig. 6a–e. It was observed that the P3HT diffraction intensity (integrated over all orientations) increases with temperature, which corresponds to the increase in the P3HT crystallinity within the films (Figure S6–S7). Furthermore, it was observed that the peak width for all peaks decreases (Figure S5). By using the Williamson-Hall approach,[32] it can be estimated that the crystallite thickness of the *a*-axis of the P3HT crystallites increases from a minimum value of 21 nm as-cast to 32 nm after annealing at 150 °C and cooling to room temperature, which corresponds to roughly 20 P3HT chains thick (Figure S3). Note that with the active layer thicknesses used in this study, the crystallites do not span the entire thickness of the BHJ film. As the temperature is increased from 90 °C to 180 °C, the diffraction intensity increases for the P3HT (020) peak (from the pi-stacking) near the meridian relative to that at the horizon at $\mathbf{q} = 1.65$ Å^{-1} (Figure S6). This increase is accompanied by an increase in the P3HT (h00) reflections near the horizon. Both of these increases in the diffraction intensity correspond to the increase in face-on oriented P3HT crystallites (Fig. 3a) and agree with the constant

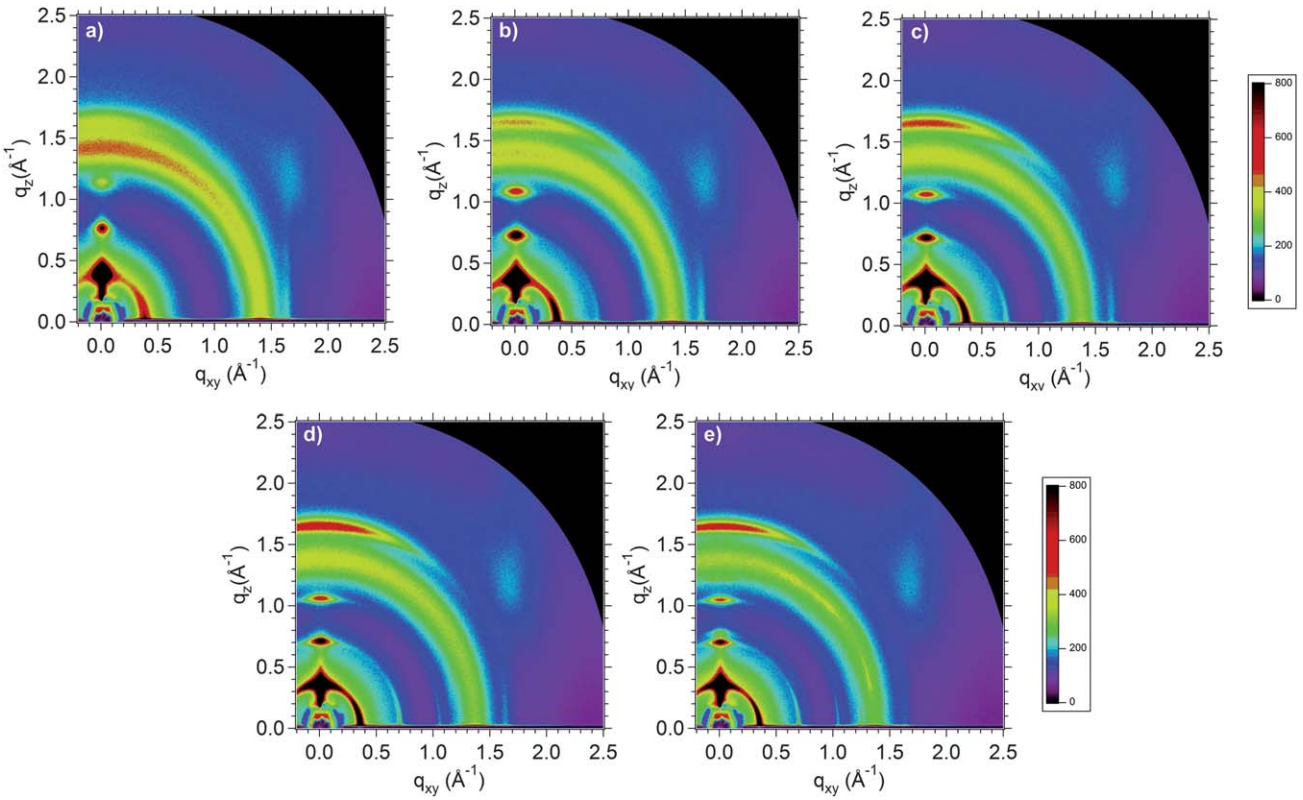

Fig. 6 Two-dimensional GIWAXS of a P3HT:PCBM BHJ a) as-cast, b) measured at 90 °C, c) 120 °C, d) 150 °C, and e) 180 °C at a rate of 30 °C min^{-1} and held every 10 °C for 4 min.

temperature measurements. At temperatures below 170 °C, there was a slight decrease in the radial scattering intensity of the ring found at $\mathbf{q} = 1.41$ Å^{-1} corresponding to highly disordered aggregates of PCBM (Figure S7c). This is consistent with previous studies showing that temperature changes the miscibility of the PCBM in the disordered regions of P3HT.[18] From this, one would expect that this change in miscibility will have an effect on the size and number of the PCBM aggregates within the blend, and thus the scattering intensity attributed to the disordered fullerene domains. However, since there is only a slight decrease in the relative intensity of the PCBM scattering, we believe that the PCBM is distributed within the BHJ film as both connected, disordered aggregates (correlation length of ~2 nm or 8 molecules in 3 dimensions) and isolated PCBM within the disordered P3HT (one or a few PCBM molecules). This is likely similar to the as-cast PCBM morphology in the P3HT:PCBM BHJ.

At 180 °C, it was observed that the diffraction peaks near the meridian at $\mathbf{q} = 0.77$ and 1.22 Å^{-1} and radially at $\mathbf{q} = 1.38$ Å^{-1} began to intensify with continued heating. These peaks originate from a crystalline form of PCBM commonly observed as needle like aggregates.[7] Optical microscopy images of the same samples (Figure S10) show that the micron-scale phase separation commonly observed is in fact crystalline domains of PCBM.[7,30]

The improvement in P3HT ordering is directly related to the improvement in the J_{sc} and FF as observed during thermal annealing, and agrees with previous reports.[4,12,13] At temperatures below 180 °C, we find no correlation between the improvement in photoconversion efficiency and the change in the molecular ordering of PCBM. At temperatures approaching 180 °C, rapid formation of micon-scale PCBM crystallites is linked to degradation in the photoconversion efficiency.[17,30] This conclusion is consistent with the recent report by Labram *et al.*, which showed that there was a decrease in the electron mobility of P3HT:PCBM field-effect transistors when heated above 140 °C.[33] In our samples, we do not find diffraction corresponding to PCBM without the observation of micron-scale domains of PCBM. Our data suggests that only micron-scale domains of PCBM crystallites are formed under these conditions, which is correlated to the decrease in device performance. Thus, it is believed that an efficient P3HT:PCBM BHJ does not require highly ordered crystalline regions of PCBM, but is comprised mainly of highly disordered aggregates of PCBM. In some publications, these domains are referred to as "nanocrystals", but based on the relatively small coherence lengths observed here, we prefer the phrase "disordered aggregate." Our conclusions disagree with those of Gomez *et al.*, who conclude that establishing local organization within the PCBM is essential for high performance P3HT:PCBM BHJ solar cells. While the origin of this discrepancy is not completely clear, it is plausible that this results from different fabrication conditions and thermal annealing temperature and times (165 °C for up to 240 h in ref. 12). However, we agree that the connectivity of these aggregates is a key feature of the transport pathway for extraction of electrons from the BHJ.[12,14]

4. Conclusions

By using complementary J–V measurements and 2D GIWAXS during annealing, it was determined that the improvement in the

molecular ordering of the P3HT component of the BHJ occurs within the first 5 min of heating, with little improvement observed thereafter. The improvement in the photoconversion efficiency was strongly correlated with the population of face-on oriented P3HT crystallites; no change in the molecular ordering of the PCBM was observed. By increasing the temperature at a constant rate, it was found that the J_{sc} increases. This increase in J_{sc} was correlated to the increase in total P3HT crystallite population and to the increase in the number of face-on oriented P3HT crystallites. Once again, very little change in the molecular ordering of the PCBM phase was observed. At longer time periods, it was found that the photoconversion efficiency decreased, which was linked to the formation of micron-scale PCBM crystallites. Thus, these results are consistent with the idea that the increase in the P3HT crystallite population (not the increase in the molecular order of the PCBM phase) is the main contributing factor to the increase in photoconversion efficiency upon thermal annealing. We believe that the PCBM is distributed within the disordered domains of P3HT as both molecularly dispersed and highly disordered aggregates of PCBM. Our scattering data does not address the interconnectivity of these highly disordered aggregates of PCBM, which is important for effective extraction of electrons.[34]

From this study, we find that *in situ* J–V measurements are a useful tool for probing changes in the power conversion efficiency of P3HT:PCBM BHJs. Using the model system, we find that thermal annealing for short times (<10 min) at 150 °C is all that is required for efficient PCE in these BHJs. Longer periods of time can result in degradation in the photoconversion efficiency due to micron-scale PCBM crystallization. These results represent a benchmark study for examining the changes in optoelectornic characteristics at elevated temperatures. We believe that the methodology outlined here will be helpful for testing new materials where the annealing time at each temperature is difficult to optimize without large numbers of samples. For example, one can easily imagine cases where times chosen for annealing are too long leading to degradation and abandonment of thermal treatment as a tool for improvement of PCE.

Acknowledgements

Portions of this work were carried out using the MRL Central Facilities, which are supported by the MRSEC Program of the NSF under Award No. DMR05-20415; a member of the NSF-funded Materials Research Facilities Network (www.mrfn.org). We thank the NSF SOLAR program for partial support of this work (CHE-1035292). Portions of this research were carried out at the SSRL, a national user facility operated by Stanford University on behalf of the U.S. Department of Energy, Office of Basic Energy Sciences. NDT acknowledges support from the ConvEne IGERT Program (NSF-DGE 0801627) and NSF Graduate Research Fellowship. CGS acknowledges support from the Center for Energy Efficient Materials, an Energy Frontier Research Center funded by the U.S. Department of Energy, Office of Science, Office of Basic Energy Sciences under Award Number DE-SC0001009. We thank Eric Verploegen for his assistance with the beam line 11–3 annealing chamber.

References

1 Y. Y. Liang, Z. Xu, J. B. Xia, S. T. Tsai, Y. Wu, G. Li, C. Ray and L. P. Yu, *Adv. Mater.*, 2010, **22**, E135–E138.
2 G. Yu, J. Gao, J. C. Hummelen, F. Wudl and A. J. Heeger, *Science*, 1995, **270**, 1789–1791.
3 M. C. Scharber, D. Wuhlbacher, M. Koppe, P. Denk, C. Waldauf, A. J. Heeger and C. L. Brabec, *Adv. Mater.*, 2006, **18**, 789–794.
4 T. Erb, U. Zhokhavets, G. Gobsch, S. Raleva, B. Stuhn, P. Schilinsky, C. Waldauf and C. J. Brabec, *Adv. Funct. Mater.*, 2005, **15**, 1193–1196.
5 Y. Kim, S. A. Choulis, J. Nelson, D. D. C. Bradley, S. Cook and J. R. Durrant, *Appl. Phys. Lett.*, 2005, **86**.
6 W. L. Ma, C. Y. Yang, X. Gong, K. Lee and A. J. Heeger, *Adv. Funct. Mater.*, 2005, **15**, 1617–1622.
7 C. H. Woo, B. C. Thompson, B. J. Kim, M. F. Toney and J. M. J. Frechet, *J. Am. Chem. Soc.*, 2008, **130**, 16324–16329.
8 P. Schilinsky, U. Asawapirom, U. Scherf, M. Biele and C. J. Brabec, *Chem. Mater.*, 2005, **17**, 2175–2180.
9 G. Li, V. Shrotriya, Y. Yao and Y. Yang, *J. Appl. Phys.*, 2005, **98**.
10 X. N. Yang, J. Loos, S. C. Veenstra, W. J. H. Verhees, M. M. Wienk, J. M. Kroon, M. A. J. Michels and R. A. J. Janssen, *Nano Lett.*, 2005, **5**, 579–583.
11 G. Dennler, M. C. Scharber and C. J. Brabec, *Adv. Mater.*, 2009, **21**, 1323–1338.
12 E. D. Gomez, K. P. Barteau, H. Wang, M. F. Toney and Y. L. Loo, *Chem. Commun.*, 2011, **47**, 436–438.
13 E. Verploegen, R. Mondal, C. J. Bettinger, S. Sok, M. F. Toney and Z. A. Bao, *Adv. Funct. Mater.*, 2010, **20**, 3519–3529.
14 T. Agostinelli, S. Lilliu, J. G. Labram, M. Campoy-Quiles, M. Hampton, E. Pires, J. Rawle, O. Bikondoa, D. D. C. Bradley, T. D. Anthopoulos, J. Nelson and J. E. Macdonald, *Adv. Funct. Mater.*, 2011, **21**, 1701–1708.
15 L. H. Nguyen, H. Hoppe, T. Erb, S. Gunes, G. Gobsch and N. S. Sariciftci, *Adv. Funct. Mater.*, 2007, **17**, 1071–1078.
16 Y.-J. Cheng, C.-H. Hsieh, P.-J. Li and C.-S. Hsu, *Adv. Funct. Mater.*, 2011, **21**, 1723–1732.
17 B. J. Kim, Y. Miyamoto, B. W. Ma and J. M. J. Frechet, *Adv. Funct. Mater.*, 2009, **19**, 2273–2281.
18 N. D. Treat, M. A. Brady, G. Smith, M. F. Toney, E. J. Kramer, C. J. Hawker and M. L. Chabinyc, *Adv. Energy Mater.*, 2011, **1**, 82–89.
19 B. Watts, W. J. Belcher, L. Thomsen, H. Ade and P. C. Dastoor, *Macromolecules*, 2009, **42**, 8392–8397.
20 J. C. Blakesley, H. S. Clubb and N. C. Greenham, *Phys. Rev. B: Condens. Matter Mater. Phys.*, 2010, **81**, 045210.
21 A. Salleo, T. W. Chen, A. R. Volkel, Y. Wu, P. Liu, B. S. Ong and R. A. Street, *Phys. Rev. B*, 2004, **70**.
22 C. Yang, F. P. Orfino and S. Holdcroft, *Macromolecules*, 1996, **29**, 6510–6517.
23 G. Li, V. Shrotriya, J. S. Huang, Y. Yao, T. Moriarty, K. Emery and Y. Yang, *Nat. Mater.*, 2005, **4**, 864–868.
24 D. Chen, A. Nakahara, D. Wei, D. Nordlund and T. P. Russell, *Nano Lett.*, 2011, **11**, 561–567.
25 J. L. Baker, L. H. Jimison, S. Mannsfeld, S. Volkman, S. Yin, V. Subramanian, A. Salleo, A. P. Alivisatos and M. F. Toney, *Langmuir*, 2010, **26**, 9146–9151.
26 N. I. Craciun, J. Wildeman and P. W. M. Blom, *Phys. Rev. Lett.*, 2008, **100**.
27 J. Zhao, A. Swinnen, G. Van Assche, J. Manca, D. Vanderzande and B. Van Mele, *J. Phys. Chem. B*, 2009, **113**, 1587–1591.
28 V. D. Mihailetchi, L. J. A. Koster and P. W. M. Blom, *Appl. Phys. Lett.*, 2004, **85**, 970–972.
29 P. E. Hopkinson, P. A. Staniec, A. J. Pearson, A. D. F. Dunbar, T. Wang, A. J. Ryan, R. A. L. Jones, D. G. Lidzey and A. M. Donald, *Macromolecules*, 2011, **44**, 2908–2917.
30 J. Jo, S. S. Kim, S. I. Na, B. K. Yu and D. Y. Kim, *Adv. Funct. Mater.*, 2009, **19**, 866–874.
31 L. Chang, H. W. A. Lademann, J.-B. Bonekamp, K. Meerholz and A. J. Moulé, *Adv. Funct. Mater.*, 2011, **21**, 1779–1787.
32 L. H. Jimison, A. Salleo, M. L. Chabinyc, D. P. Bernstein and M. F. Toney, *Phys. Rev. B: Condens. Matter Mater. Phys.*, 2008, **78**.
33 J. G. Labram, E. B. Domingo, N. Stingelin, D. D. C. Bradley and T. D. Anthopoulos, *Adv. Funct. Mater.*, 2011, **21**, 356–363.
34 B. C. Thompson and J. M. J. Frechet, *Angew. Chem., Int. Ed.*, 2008, **47**, 58–77.